

Formation of Giant Planets by Disk Instability on Wide Orbits Around Protostars with Varied Masses

Alan P. Boss

*Department of Terrestrial Magnetism, Carnegie Institution of Washington, 5241 Broad
Branch Road, NW, Washington, DC 20015-1305*

boss@dtm.ciw.edu

ABSTRACT

Doppler surveys have shown that more massive stars have significantly higher frequencies of giant planets inside ~ 3 AU than lower mass stars, consistent with giant planet formation by core accretion. Direct imaging searches have begun to discover significant numbers of giant planet candidates around stars with masses of $\sim 1 M_{\odot}$ to $\sim 2 M_{\odot}$ at orbital distances of ~ 20 AU to ~ 120 AU. Given the inability of core accretion to form giant planets at such large distances, gravitational instabilities of the gas disk leading to clump formation have been suggested as the more likely formation mechanism. Here we present five new models of the evolution of disks with inner radii of 20 AU and outer radii of 60 AU, for central protostars with masses of 0.1, 0.5, 1.0, 1.5, and $2.0 M_{\odot}$, in order to assess the likelihood of planet formation on wide orbits around stars with varied masses. The disk masses range from $0.028 M_{\odot}$ to $0.21 M_{\odot}$, with initial Toomre Q stability values ranging from 1.1 in the inner disks to ~ 1.6 in the outer disks. These five models show that disk instability is capable of forming clumps on time scales of $\sim 10^3$ yr that, if they survive for longer times, could form giant planets initially on orbits with semimajor axes of ~ 30 AU to ~ 70 AU and eccentricities of ~ 0 to ~ 0.35 , with initial masses of $\sim 1M_{Jup}$ to $\sim 5M_{Jup}$, around solar-type stars, with more protoplanets forming as the mass of the protostar (and protoplanetary disk) are increased. In particular, disk instability appears to be a likely formation mechanism for the HR 8799 gas giant planetary system.

Subject headings: accretion, accretion disks – hydrodynamics – instabilities – planetary systems: formation – solar system: formation

1. Introduction

Direct imaging searches for extrasolar planets have typically placed only upper limits on the frequency of giant planets on orbits between ~ 20 AU and ~ 100 AU (Nielson et al. 2008; Nielsen & Close 2010) or ~ 40 AU and ~ 200 AU (Lafrenière et al. 2007), for planets with masses above $4 M_{Jup}$ or $2 M_{Jup}$, respectively. These surveys led to upper limits on the frequency of giant planet companions on such orbits of $\sim 10\%$ to $\sim 20\%$. These upper limits are, however, comparable to estimates of the frequency of detected giant planets on orbits inside ~ 3 AU of FGKM dwarfs by Doppler spectroscopy (Cumming et al. 2008). Gravitational microlensing detections of ice and gas giant planets orbiting beyond 3 AU imply an even higher frequency of planets, about 35% (Gould et al. 2010). Hence, significant numbers of giant planets on wide orbits might very well exist.

Recently, persuasive evidence has begun to appear that wide giant planets do indeed exist in significant numbers. The A3V star ($2.06 M_{\odot}$) Fomalhaut appears to have a planetary companion 119 AU away with a mass less than $3 M_{Jup}$, based on the planet’s failure to disrupt the cold dust belt in which it is embedded (Kalas et al. 2008). The A5V star ($1.5 M_{\odot}$) HR 8799 appears to have a system of at least four gas giant planets, orbiting at projected distances of 14, 24, 38, and 68 AU, with minimum masses of 7, 7, 7, and $5 M_{Jup}$, respectively, based on their luminosities and an estimated age of the system of 30 Myr (Marois et al. 2008, 2010). The four HR 8799 exoplanets are also embedded in a dust debris disk (Su et al. 2009). A companion with a mass in the range of 10 to $40 M_{Jup}$ has been detected at a projected separation of 29 AU from the G9 star ($0.97 M_{\odot}$) GJ 758 (Thalmann et al. 2009), and other good candidates for wide planetary companions have been proposed as well (e.g., Oppenheimer et al. 2008; Lafrenière, Jayawardhana, & van Kerkwijk 2008). Heinze et al. (2010a,b), however, estimate that no more than 8.1% of the 54 sun-like stars studied in their planet imaging survey could have planets similar to those of HR 8799.

Doppler surveys have been extended to a range of stellar masses, providing the first estimates of how the planetary census depends on stellar type. A-type stars appear to have a significantly higher frequency of giant planets with orbits inside 3 AU compared to solar-type stars (Bowler et al. 2010). M dwarfs, on the other hand, appear to have a significantly lower frequency of giant planets inside 2.5 AU than FGK dwarfs (Johnson et al. 2010). Thus there is a clear indication that the frequency of giant planets increases with stellar mass, at least for relatively short period orbits. Assuming that protoplanetary disk masses increase with increasing stellar mass, such a correlation is consistent with the core accretion mechanism for giant planet formation, as a higher surface density of solids leads to proportionately larger mass cores that could become gas giant planets (e.g., Wetherill 1996; Ida & Lin 2005). However, microlensing detections (Gould et al. 2010) imply a considerably

higher frequency ($\sim 35\%$) of giant planets around early M dwarf stars ($\sim 0.5M_{\odot}$) than that found by the Doppler surveys, again orbiting at larger distances than those probed by the Doppler surveys. Evidently even early M dwarfs might also have a significant population of relatively wide gas giant planets.

Core accretion is unable, however, to form massive planets beyond ~ 35 AU, even in the most favorable circumstances (e.g., Levison & Stewart 2001; Thommes, Duncan, & Levison 2002; Chambers 2006), and gravitational scattering outward appears to be unable to lead to stable wide orbits (Dodson-Robinson et al. 2009; Raymond, Armitage, & Gorelick 2010). Disk instability (Boss 1997) is then the remaining candidate mechanism for forming wide gas giant planets (Dodson-Robinson et al. 2009; Boley 2009). Previous models found that disk instability could readily produce giant planets at distances of 20 AU to 30 AU (Boss 2003), but not at distances of 100 AU to 200 AU (Boss 2006a). Here we present results for intermediate-size disks (20 AU to 60 AU) for a range of central protostar masses (0.1 to $2.0 M_{\odot}$), to learn if the disk instability mechanism for giant planet formation is consistent with the results of the Doppler and direct imaging surveys to date.

2. Numerical Methods

The calculations were performed with a numerical code that solves the three dimensional equations of hydrodynamics and radiative transfer in the diffusion approximation, as well as the Poisson equation for the gravitational potential. This same basic code has been used in all of the author’s previous studies of disk instability. The code is second-order-accurate in both space and time. A complete description of the entire code, including hydrodynamics and radiative transfer, may be found in Boss & Myhill (1992), with the following exceptions: The central protostar is assumed to move in such a way as to preserve the location of the center of mass of the entire system (Boss 1998), which is accomplished by altering the location of the point mass source of the star’s gravitational potential to balance the center of mass of the disk. The Pollack et al. (1994) Rosseland mean opacities are used for the dust grains that dominate the opacities in these models. The energy equation of state in use since 1989 is described by Boss (2007). A flux-limiter for the diffusion approximation radiative transfer was not employed, as it appears to have only a modest effect on midplane temperatures (Boss 2008). Recent tests of the radiative transfer scheme are described in Boss (2009).

The equations are solved on a spherical coordinate grid with $N_r = 101$ (including the central grid cell, which contains the central protostar), $N_{\theta} = 23$ in $\pi/2 \geq \theta \geq 0$, and $N_{\phi} = 256$, with N_{ϕ} being increased to 512 once fragments begin forming. The radial grid is uniformly spaced with $\Delta r = 0.4$ AU between 20 and 60 AU. The θ grid is compressed

into the midplane to ensure adequate vertical resolution ($\Delta\theta = 0.3^\circ$ at the midplane). The ϕ grid is uniformly spaced. The number of terms in the spherical harmonic expansion for the gravitational potential of the disk is $N_{Ylm} = 32$ when $N_\phi = 256$, while $N_{Ylm} = 48$ when $N_\phi = 512$.

The Jeans length criterion (e.g., Boss et al. 2000) and the Toomre length criterion (Nelson 2006) are both monitored throughout the evolutions to ensure that any clumps that might form are not numerical artifacts. The Jeans length criterion consists of requiring that all of the grid spacings in the spherical coordinate grid remain smaller than 1/4 of the Jeans length $\lambda_J = \sqrt{\frac{\pi c_s^2}{G\rho}}$, where c_s is the local sound speed, G the gravitational constant, and ρ the density. Similarly, the Toomre length criterion consists of requiring that all of the grid spacings remain smaller than 1/4 of the Toomre length $\lambda_T = (2c_s^2/G\Sigma)$, where Σ is the mass surface density. Once well-defined fragments form, these criteria may be violated at the maximum densities of the clumps, due to the non-adaptive nature of the spherical coordinate grid, as is expected to be the case for self-gravitating clumps that are trying to contract to higher densities on a fixed grid. However, provided that the Jeans and Toomre constraints are satisfied at the time that well-defined clumps appear, these clumps are expected to be genuine and not spurious artifacts.

The boundary conditions are chosen at both 20 and 60 AU to absorb radial velocity perturbations, to simulate the continued existence of the disk inside and outside the active numerical grid. As discussed in detail by Boss (1998), the use of such non-reflective boundary conditions should err on the side of caution regarding the growth of perturbations, as found by Adams, Ruden, & Shu (1989). Mass and momentum that enters the innermost shell of cells at 20 AU are added to the central protostar, whereas mass or momentum that reaches the outermost shell of cells at 60 AU remains on the active hydrodynamical grid.

The controversy over whether or not disk instability can lead to protoplanet formation inside about 20 AU continues unabated (see the recent reviews by Durisen et al. 2007 and Mayer, Boss, & Nelson 2010). Attempts to find a single reason for different numerical outcomes for disk instability models have been largely unsuccessful to date (e.g., Boss 2007, 2008), implying that the reason cannot be traced to a single code difference, but rather to the totality of differences, such as spatial resolution, gravitational potential accuracy, artificial viscosity, stellar irradiation effects, radiative transfer, numerical heating, equations of state, initial density and temperature profiles, disk surface boundary conditions, and time step size, to name a few.

Comparison calculations on nearly identical disk models have led Boss (2007) and Cai et al. (2010) to reach different conclusions. While Boss (2007) concluded that fragmentation was possible inside 20 AU, Cai et al. (2010) found no evidence for fragmentation in their

models, which included numerous improvements over their previous work, such as a better treatment of radiative transfer in optically thin regions of the disk and elimination of the spurious numerical heating in the inner disk regions where Boss (2007) found fragments to form. Cai et al. (2010) suggested that the main difference might be artificially fast cooling in the Boss models as a result of the thermal bath boundary conditions used in Boss models, which could not be duplicated with the Cai et al. (2010) code because of numerical stability problems. Analytical test cases have been advanced as one means for testing radiative transfer in the numerical codes (e.g., Boley et al. 2006). Boss (2009) derived two new analytical radiative transfer solutions and showed that Boss code does an excellent job of handling the radiative boundary conditions of a disk immersed in a thermal bath; the Boss code relaxes to the analytical solutions for both a spherically symmetric cloud and an axisymmetric disk.

Recently, Boss (2010) published models showing that disk instability is considerably less robust inside 20 AU in disks with half the mass of previous models (e.g., Boss 2007), but still possible. Inutsuka, Machida, & Matsumoto (2010) found in their magnetohydrodynamic collapse calculations that the massive disks that formed were subject to gravitational instability and fragment formation, even inside 20 AU. Arguments against inner disk fragmentation are often based on simple cooling time estimates (e.g., Cai et al. 2010). However, Meru & Bate (2010, 2011) have emphasized that many previous numerical calculations with fixed cooling times are likely to have reached incorrect results, in part as a result of insufficient spatial resolution. Meru & Bate (2010, 2011) presented numerous disk instability models that underwent fragmentation inside 20 AU for a variety of initial conditions. While the debate over inner disk fragmentation is likely to continue, the present models should be considerably less controversial, given their restriction to fragmentation at distances greater than 20 AU.

3. Initial Conditions

Table 1 lists the initial conditions chosen for the five disk models presented here. Models 2.0, 1.5, 1.0, 0.5, and 0.1 depict disks around protostars with masses of $M_s = 2.0, 1.5, 1.0, 0.5$, and $0.1 M_\odot$, representing future A3, A5, G2, early M, and late M dwarfs, respectively, depending on their subsequent accretion of mass. The disk envelopes are taken to have temperatures (T_e) between 50 K and 30 K, in all cases hotter than the disks themselves, which begin their evolutions uniformly isothermal at the initial temperatures (T_i) shown in Table 1. The critical density for differentiating between the disk and the disk envelope is taken to be $10^{-13} \text{ g cm}^{-3}$ for models 2.0, 1.5, 1.0, and 0.5, and $10^{-14} \text{ g cm}^{-3}$ for model 0.1, which effectively determines the onset of the envelope thermal bath. Variations in these

parameters have been tested by Boss (2007) and found to have relatively minor effects.

Envelope temperatures of 30 to 50 K appear to be reasonable bounds for low-mass protostars during quiescent periods (Chick & Cassen 1997). Observations of the DM Tau outer disk, on scales of 50 to 60 AU, imply midplane temperatures of 13 to 20 K (Dartois, Dutrey, & Guilloteau 2003). Hence the envelope and disk initial temperatures chosen in Table 1 appear to be reasonable choices for real disks.

Initially the disks have the density distribution (Boss 1993) of an adiabatic, self-gravitating, thick disk in near-Keplerian rotation about a stellar mass M_s

$$\rho(R, Z)^{\gamma-1} = \rho_o(R)^{\gamma-1} - \left(\frac{\gamma-1}{\gamma}\right) \left[\left(\frac{2\pi G \sigma(R)}{K}\right) Z + \frac{GM_s}{K} \left(\frac{1}{R} - \frac{1}{(R^2 + Z^2)^{1/2}}\right) \right],$$

where R and Z are cylindrical coordinates, $\rho_o(R)$ is the midplane density, and $\sigma(R)$ is the surface density. The adiabatic constant is $K = 1.7 \times 10^{17}$ (cgs units) and $\gamma = 5/3$ for the initial model; thereafter, the disk evolves in a nonisothermal manner governed by the energy equation and radiative transfer (Boss & Myhill 1992). The first adiabatic exponent (Γ_1) derived from the energy equation of state for these models varies from $5/3$ for temperatures below 100 K to ~ 1.4 for higher temperatures (see Figure 1 in Boss 2007). The radial variation of the initial midplane density is a power law that ensures near-Keplerian rotation throughout the disk

$$\rho_o(R) = \rho_{o4} \left(\frac{R_4}{R}\right)^{3/2},$$

where $\rho_{o4} = (M_s/M_\odot) \times 10^{-10}$ g cm $^{-3}$ and $R_4 = 4$ AU. This disk structure is the continuation to 60 AU of the same disk used in the $M_s = 1.0M_\odot$ models of, e.g., Boss (2001, 2003, 2005, 2006a, 2010). While each disk is initially close to centrifugal balance in the radial direction, the use of the Boss (1993) analytical density distribution, with varied initial disk temperatures, means that the disks initially contract vertically until a quasi-equilibrium state is reached (Boss 1998).

Table 1 lists the resulting disk masses M_d (from 20 AU to 60 AU), the disk mass to stellar mass ratios M_d/M_s , the initial disk temperatures T_i , and the initial minimum and maximum values of the Toomre (1964) Q gravitational stability criterion, increasing monotonically outward from unstable $Q = 1.1$ values at 20 AU to marginally stable $Q \sim 1.6$ at 60 AU. These values of Q were chosen to be low enough in the inner disk regions to err on the side of clump formation; higher initial Q values are expected to stifle disk fragmentation.

These models thus represent a first exploration of parameter space for large-scale disks to establish feasibility. Further work should investigate higher Q initial conditions, as disks are expected to evolve starting from marginally gravitationally unstable ($Q > 1.5$) initial conditions (e.g., Boley 2009). Such disks typically also fragment, but only after a period of dynamical evolution toward $Q \sim 1$ in limited regions, such as dense rings (e.g., Boss 2002).

Large, massive disks have been detected in regions of low-mass star formation, such as the 300-AU-scale, $\sim 1M_{\odot}$ disk around the class O protostar Serpens FIRS 1 (Enoch et al. 2009). Observations of 11 low- and intermediate-mass pre-main-sequence stars imply that their circumstellar disks formed with masses in the range from $0.05 M_{\odot}$ to $0.4 M_{\odot}$ (Isella, Carpenter, & Sargent 2009). These and other observations support the choice of the disk masses and sizes assumed in the present models.

4. Results

All of the models dynamically evolve in much the same way. Beginning from nearly axisymmetric configurations (with initial $m = 1, 2, 3, 4$ density perturbations of amplitude 1%), the disks develop increasingly stronger spiral arm structures. Eventually these trailing spiral arms become distinct enough, through self-gravitational growth and mutual collisions, that reasonably well-defined clumps appear and maintain their identities for some fraction of an orbital period. However, because the fixed-grid nature of these calculations prevents the clumps from contracting to much higher densities, the clumps are doomed to eventual destruction by a combination of thermal pressure, tidal forces from the protostar, and Keplerian shear. However, new clumps continue to form and orbit the protostar, suggesting that clump formation is inevitable. Previous work (Boss 2005) has shown that as the numerical spatial resolution is increased, the survival of clumps formed by disk instability is enhanced. While an adaptive-mesh-refinement code would be desirable for demonstrating that clumps can contract and survive, the present models, combined with the previous work by Boss (2005), are sufficient for a first exploration of this region of disk instability parameter space.

Figures 1 through 10 show the midplane density and temperature contours for all five models at a time of $\sim 6P_{20}$, where P_{20} is the Keplerian orbital period at the distance of the inner grid boundary of 20 AU for a protostar with the given mass. For models 0.1, 0.5, 1.0, 1.5, and 2.0, respectively, P_{20} is equal to 283 yr, 126 yr, 89.4 yr, 73.0 yr, and 63.2 yr. It is clear that clumps have formed by this time in all five models. However, in order to become a giant planet, clumps must survive long enough to contract toward planetary densities. The spherically symmetric protoplanet models of Helled & Bodenheimer (2011) suggest contraction time scales ranging from $\sim 10^3$ yr to $\sim 10^5$ yr, depending on the metallicity, for

protoplanets with masses from 3 to 7 M_{Jup} , so these clumps must survive for many orbital periods in order to become planets.

Table 2 lists the estimated properties for those clumps that appear to be self-gravitating at the earlier time of $\sim 4P_{20}$, while Table 3 lists the estimates for the fragments at the time of $\sim 6P_{20}$ depicted in Figures 1 through 10. At both of these times, clump formation was relatively well-defined, so that the clump masses and other properties could be estimated. Clumps typically first become apparent at $\sim 2P_{20}$. Candidate clumps are identified by eye from the equatorial density contour plots, and then interrogated with a program that allows the user to select cells adjoining the cell with the maximum density in order to achieve a candidate clump with an approximately spherical appearance, in spite of the obvious banana-shape of many clumps. The fragment masses M_{frag} are then estimated in units of the Jupiter mass M_{Jup} and compared to the Jeans mass M_{Jeans} (e.g., Spitzer 1968) necessary for gravitational stability at the mean density and temperature of the fragment. Fragments with masses less than the Jeans mass are not expected to be stable (Boss 1997).

The times presented in Figures 1 through 10 range from 387 yr to 1843 yr, i.e., timescales of order 1000 yr. Compared to core accretion, where the time scales involved are measured typically in millions of yr (e.g., Ida & Lin 2005) and low mass stars are in danger of not being able to form gas giant planets at all (Laughlin, Bodenheimer, & Adams 2004), the disks around even low mass stars are able to form clumps on time scales short enough to permit gas giant protoplanet formation to occur in the shortest-lived protoplanetary disks.

Figures 1 through 10 demonstrate that while clump formation occurs for all of the disks, the clumps that form becoming increasingly numerous as the mass of the protostar (and of the corresponding disk) increases, even though all disks begin their evolution with essentially the same range of Toomre (1964) Q values. Clearly more massive disks are able to produce more numerous protoplanets, all other things being equal. The temperature contour plots show that significant compressional heating occurs in these initially isothermal disks as a result of spiral arm formation, with the most significant heating occurring near the edges of the arms and clumps, as more disk gas seeks to infall onto the spiral structures; the local temperature maxima do not necessarily fall at the local density maxima. A similar effect was found by Boley & Durisen (2008). This suggests that clump formation in these relatively cold outer disks occurs in an opportunistic manner, pulling cold disk gas together wherever possible. Even the lowest mass disk in model 0.1 is optically thick, with a vertical optical depth of ~ 5 , while vertical optical depths of $\sim 10^3$ characterize the more massive disks, so some combination of vertical radiation transport, dynamical motions, and/or convection (e.g., Boss 2004, Boley & Durisen 2006, Mayer et al. 2007) is necessary for cooling the disk midplane and allowing the clumps to continue their contraction toward planetary densities.

Tables 2 and 3 also list the estimated orbital semimajor axes a_{frag} and eccentricities e_{frag} for the fragments at the same times as the other fragment properties are estimated. Needless to say, these values should be taken solely as initial values, as interactions with the massive disk (e.g., Boss 2005) and the other fragments will result in substantial further orbital evolution. The fragment orbital parameters a and e were calculated using each fragment’s radial distance r , average radial velocity v_r , and average azimuthal velocity v_ϕ (both derived from the total momentum of the clump), along with the model’s stellar mass M_s , and inserting these values into these equations for a body on a Keplerian orbit (Danby 1988):

$$a = \frac{GM_s}{2} \left(\frac{GM_s}{r} - \frac{v_r^2}{2} - \frac{v_\phi^2}{2} \right)^{-1},$$

$$e = \left(1 - \frac{r^2 v_\phi^2}{GM_s a} \right)^{1/2},$$

where G is the gravitational constant.

Figures 11 and 12 depict the midplane density and temperature profiles for two of the clumps that form in model 1.0, as shown in Figures 5 and 6. The fragment in Figure 11 is less well-defined than that in Figure 12, yet still has an estimated mass of $3.8 M_{Jup}$, well above its relevant Jeans mass of $1.8 M_{Jup}$. The fragment in Figure 12 has an estimated mass of $2.5 M_{Jup}$, also well above its relevant Jeans mass of $2.2 M_{Jup}$. These figures show that the higher density fragment in Figure 12 has resulted in a higher temperature interior, while the lower density fragment in Figure 11 has not yet reached similar internal temperatures, though in both cases the maximum fragment temperatures occur close to their edges. Similar plots characterize all of the fragments found in these models.

Figures 13, 14, 15, and 16 plot the resulting estimates of the initial protoplanet masses, semimajor axes, and eccentricities as a function of protostar or protoplanetary disk mass, for the fragments in Tables 2 and 3 where the fragment mass is equal to or greater than the Jeans mass. Given the uncertain future evolution of the fragments as they attempt to survive and become true protoplanets, these values should be taken only as reasonable estimates based on the present set of models, subject to the inherent assumptions about the initial disk properties. Boley et al. (2010), for example, found that clumps on highly eccentric orbits could be tidally disrupted at periastron. In addition, surviving fragments are likely to gain substantially more disk gas mass during their orbital evolution (“type IV non-migration”) in a marginally gravitationally unstable disk (Boss 2005). Nevertheless, Figure 13 makes it clear that disk instability is capable of leading to gas giant protoplanet formation around

protostars with masses in the range from 0.1 to 2.0 M_{\odot} , with more protoplanets forming as the mass of the protostar and its disk increases: perhaps only a single protoplanet for a 0.1 M_{\odot} protostar, but as many as six for a 2.0 M_{\odot} protostar. The masses of the protoplanets appear to increase with the stellar and disk mass (Figures 13 and 14); the typical initial protoplanet mass increased from $\sim 1M_{Jup}$ to $\sim 3M_{Jup}$ over the range of models 0.1 to 2.0.

Given the large disk masses, it is likely that the final protoplanet masses will similarly increase with time, as those protoplanets accrete mass from a massive reservoir of gas and dust. This growth will be limited though by the angular momentum of the disk gas that the protoplanet is trying to accrete (Boley et al. 2010). Nevertheless, if one wishes to use these models to explain the formation of giant planets with minimum masses similar to those estimated for HR 8799, i.e., 5 to 7 M_{Jup} , then the outer disk gas must be removed prior to growth of the protoplanets to unacceptably large masses. Photoevaporation of the outer disk by FUV and EUV fluxes from nearby massive (OB) stars is a likely means for achieving this timely disk gas removal, on a time scale of $\sim 10^5$ yr (e.g., Balog et al. 2008; Mann & Williams 2009, 2010). If the A5V star HR 8799 formed in a region of high mass star formation, as in the case for the majority of stars, the outer disk gas should disappear within $\sim 10^5$ yr. If giant protoplanets cannot accrete mass from the disk at a rate higher than $\sim 10^{-4}M_{Jup} \text{ yr}^{-1}$, as argued by Nelson & Benz (2003), then the maximum amount of disk gas that could be accreted in 10^5 yr or less would be $\sim 10M_{Jup}$. A mass gain no greater than this appears to be roughly consistent with the range of masses estimated for the four planets in HR 8799 (Marois et al. 2008, 2010), which could be as high as 13 M_{Jup} .

Figures 15 and 16 show that these protoplanets begin their existence with orbital semi-major axes in the range of ~ 30 AU to ~ 70 AU and orbital eccentricities from ~ 0 to ~ 0.35 . Only upper limits of ~ 0.4 exist for the orbital eccentricities of the HR 8799 system (Figure 16), comfortably above the model estimates. The initial orbital eccentricities appear to vary slightly with stellar mass, with eccentricities dropping as the stellar mass increases, though this hint is largely due to the higher eccentricities found in model 0.1. The semimajor axes show a similar slight trend of decreasing with stellar mass, though both of these effects may be more of a result of small number statistics than of any robust physical mechanism at work.

Just as there is a danger that protoplanets formed in a massive disk could grow to become brown dwarfs, unless prevented from doing so by removal of the outer disk gas through photoevaporation, there is a danger that the protoplanets might suffer inward orbital migration due to interactions with the disk gas prior to its removal. However, models of the interactions of protoplanets with marginally gravitationally unstable disks (Boss 2005) have shown that the protoplanets experience an orbital evolution that is closer to a random walk

(type IV non-migration) than to the classic monotonically inward (or outward) evolution due to type II migration, where the planet clears a gap in the disk and then must move in the same direction as the surrounding disk gas. Hence, the outer disk protoplanets formed in these models need not be expected to suffer major inward or outward migration prior to photoevaporation of the outer disk, though clearly this possibility is deserving of further study.

The close-packing in semimajor axis of the fragments in model 2.0 (Figures 9 and 15) makes it clear that these protoplanets will interact gravitationally with each other (as well as with the much more massive disk), resulting in mutual close encounters and scattering of protoplanets to orbits with larger and smaller semimajor axes than their initial values (Figure 15). The evolution during this subsequent phase is best described with a fixed-grid code by using the virtual protoplanet technique, where the fragments are replaced by point mass objects that orbit and interact with the disk and each other (Boss 2005). Models that continue the present models with the virtual protoplanet technique are now underway and will be presented in a future paper.

5. Discussion

Most disk instability models have focused on forming giant planets similar to those in our Solar System, and hence have studied disks with outer radii of 20 AU (e.g., Boss 2001; Mayer et al. 2007). Boss (2003) found that disk instability could lead to the formation of self-gravitating clumps with initial orbital semimajor axes of ~ 20 AU in disks with outer radii of 30 AU. On the other hand, Boss (2006a) found no strong tendency for clump formation in disks extending from 100 AU to 200 AU. In both cases these models assumed $1 M_{\odot}$ central protostars. Model 1.0 in the present work shows that when the disk is assumed to extend from 20 AU to 60 AU, clumps are again expected to be able to form, with initial semimajor axes of ~ 30 AU to ~ 45 AU (Figure 15). Taken together, these models imply that for a $1 M_{\odot}$ protostar at least, disk instability might be able to form gaseous protoplanets with initial semimajor axes anywhere inside ~ 50 AU. When multiple protoplanets form, as is likely to be the case for stars more massive than M dwarfs, subsequent gravitational interactions are likely to result in at least a few protoplanets being kicked out to orbits with semimajor axes greater than 50 AU.

Other authors have also considered the evolution of gravitationally unstable disks with outer radii much greater than 20 AU. Stamatellos & Whitworth (2009a,b) used a smoothed particle hydrodynamics (SPH) code with radiative transfer in the diffusion approximation to model the evolution of disk instabilities in disks with the same mass as the central protostar:

$M_d = M_s = 0.7M_\odot$. The disks extended from 40 AU to 400 AU, with initial Toomre Q values of 0.9 throughout, making them initially highly gravitationally unstable. As expected, these disks rapidly fragmented into multiple clumps, which often grew to brown dwarf masses (i.e., greater than $13 M_{Jup}$) or higher, with final orbital radii as large as 800 AU. Their results are in general agreement with the present results, though the major differences in the initial disk assumptions preclude a detailed comparison.

Boley et al. (2010) used an SPH code to demonstrate multiple fragment formation at distances from ~ 50 AU to ~ 100 AU from a $0.3 M_\odot$ star in a disk with a radius of 510 AU and a mass of $0.19 M_\odot$. Given the large disk mass to stellar mass ratio of 0.63, the formation of several clumps with initial masses of $3.3 M_{Jup}$ and $1.7 M_{Jup}$ is basically consistent with the present results for model 0.5.

The result that clump formation depends on protostellar mass, with models 0.1 and 0.5 forming fewer clumps than models 1.0, 1.5, and 2.0, is consistent with the results presented by Boss (2006b), who studied the evolution of disks with outer radii of 20 AU around protostars with masses of $0.1 M_\odot$ and $0.5 M_\odot$. Boss (2006b) found that clumps could form for both protostar masses, but that while several clumps formed for the $0.5 M_\odot$ protostar, typically only a single clump formed for the $0.1 M_\odot$ protostar, similar to the results in models 0.1 and 0.5 for much larger radii disks. Thus, while not zero, the chances for giant planet formation by disk instability appear to decrease with stellar mass in the range of $0.5 M_\odot$ to $0.1 M_\odot$. A simple explanation for this outcome may be that given the assumption of disk masses that scale with protostellar masses, the number of Jupiter-mass protoplanets that could form by disk instability increases with the number of Jupiter-masses of disk gas available for their formation: e.g., the disk mass for model 2.0 is taken to be 7.5 times that of model 0.1.

Nero & Bjorkman (2009) used analytical models to study fragmentation in suitably massive protoplanetary disks, finding that their estimated cooling times were over an order of magnitude shorter than those estimates previously by Rafikov (2005), a result consistent with that of Boss (2005). Nero & Bjorkman (2009) found that the outermost planet around HR 8799 was likely to have formed by a disk instability, but that the two closer-in planets were not, a conclusion at odds with the results of the present numerical calculations. The different outcomes appear to be a result of different assumptions about the initial disk density and temperature profiles, dust grain opacities, and use of a cooling time argument rather than detailed radiative transfer and hydrodynamics. Recently the use of cooling times to depict the thermodynamics of protoplanetary disks has been called in question by the three dimensional hydrodynamical models of Meru & Bate (2010, 2011), who found that previous calculations relied on an overly simplistic cooling time argument, and that when sufficiently high spatial resolution was employed, even disks previously thought to be stable underwent

fragmentation into clumps.

Finally, it is interesting to note an observational prediction. Helled & Bodenheimer (2010) have modeled the capture of solids by gas giant protoplanets formed at distances similar to those of the four planet candidates in HR 8799 (Marois et al. 2008, 2010). They found that because such massive protoplanets contract rapidly on time scales of only $\sim 10^4$ yr, few planetesimals can be captured by gas drag in their outer envelopes, leading to a prediction that the bulk compositions of these four objects should be similar to that of their host stars if they formed by disk instability. HR 8799 has a low metallicity ($[M/H] = -0.47$; Gray & Kaye 1999), so the HR 8799 objects are expected to be similarly metal-poor, unless the protoplanets are able to form in a dust-rich region of the disk (Boley & Durisen 2010).

6. Conclusions

The present set of models has shown that disk instability is capable of the rapid formation of giant planets on relatively wide orbits around protostars with masses in the range from $0.1 M_{\odot}$ to $2.0 M_{\odot}$. While the number of protoplanets formed by disk instability appears to increase with the mass of the star (and hence of the assumed protoplanetary disk), even late M dwarf stars might be able to form gas giants on wide orbits, provided that suitably gravitationally unstable disks exist in orbit around them. These results suggest that direct imaging searches for gas giant planets on wide orbits around low mass stars are likely to continue to bear fruit; the protoplanet candidates detected to date do not appear to be rare oddballs unexplainable by theoretical models of planetary system formation. HR 8799’s four planets in particular appear to be broadly consistent with formation by disk instability, though clearly further study of the formation of this key planetary system is warranted.

I thank the two referees and the scientific editor, Eric Feigelson, for valuable improvements to both the manuscript itself, and, more importantly, to the choice of initial conditions for the models, Sandy Keiser for computer systems support, and John Chambers for advice on orbit determinations. This research was supported in part by NASA Planetary Geology and Geophysics grant NNX07AP46G, and is contributed in part to NASA Astrobiology Institute grant NNA09DA81A. The calculations were performed on the flash cluster at DTM.

REFERENCES

- Adams, F. C., Ruden, S. P., & Shu, F. H. 1989, *ApJ*, 347, 959
- Balog, Z., Rieke, G. H., Muzerolle, J., Bally, J., Su, K. Y. L., Misselt, K., & Gáspár, A.

- 2008, ApJ, 688, 408
- Boley, A. C. 2009, ApJ, 695, L53
- Boley, A. C., & Durisen, R. H. 2006, ApJ, 641, 534
- Boley, A. C., & Durisen, R. H. 2008, ApJ, 685, 1193
- Boley, A. C., & Durisen, R. H. 2010, ApJ, 724, 618
- Boley, A. C., Mejía, A. C., Durisen, R. H., Cai, K., Pickett, M. K., & D’Alessio, P. 2006, ApJ, 651, 517
- Boley, A. C., Durisen, R. H., Nordlund, A., & Lord, J. 2007, ApJ, 665, 1254
- Boley, A. C., et al. 2010, Icarus, 207, 509
- Boss, A. P. 1993, ApJ, 417, 351
- Boss, A. P. 1997, Science, 276, 1836
- Boss, A. P. 1998, ApJ, 503, 923
- Boss, A. P. 2001, ApJ, 563, 367
- Boss, A. P. 2002, ApJ, 576, 462
- Boss, A. P. 2003, ApJ, 599, 577
- Boss, A. P. 2004, ApJ, 610, 456
- Boss, A. P. 2005, ApJ, 629, 535
- Boss, A. P. 2006a, ApJ, 637, L137
- Boss, A. P. 2006b, ApJ, 643, 501
- Boss, A. P. 2007, ApJ, 661, L73
- Boss, A. P. 2008, ApJ, 677, 607
- Boss, A. P. 2009, ApJ, 694, 107
- Boss, A. P. 2010, ApJ, 725, L145
- Boss, A. P., & Myhill, E. A. 1992, ApJS, 83, 311
- Boss, A. P., Fisher, R. T., Klein, R. I., & McKee, C. F. 2000, ApJ, 528, 325
- Bowler, B. P., et al. 2010, ApJ, 709, 396
- Cai, K., Pickett, M. K., Durisen, R. H., & Milne, A. M. 2010, ApJ, 716, L176
- Chambers, J. E. 2006, ApJL, 652, L133
- Chick, K. M., & Cassen, P. 1997, ApJ, 477, 398

- Cumming, A., et al. 2008, *PASP*, 120, 531
- Danby, J. M. A. 1988, *Fundamentals of Celestial Mechanics* (Richmond, Virginia: Willman-Bell), 63
- Dartois, E., Dutrey, A., & Guilloteau, S. 2003, *A&A*, 399, 773
- Dodson-Robinson, S. E., Veras, D., Ford, E. B., & Beichman, C. A. 2009, *ApJ*, 707, 79
- Durisen, R. H., Boss, A. P., Mayer, L., Nelson, A., Rice, K., & Quinn, T. R. 2007, in *Protostars and Planets V*, B. Reipurth, D. Jewitt, & K. Keil, eds. (Tucson: University of Arizona Press), 607
- Enoch, M. L., Corder, S., Dunham, M. M., & Duchêne, G. 2009, *ApJ*, 707, 103
- Gould, A. et al. 2010, *ApJ*, submitted
- Gray, R. O., & Kaye, A. B. 1999, *AJ*, 118, 2993
- Heinze, A. N., et al. 2010a, *ApJ*, 714, 1551
- Heinze, A. N., et al. 2010b, *ApJ*, 714, 1570
- Helled, R., & Bodenheimer, P. 2010, *Icarus*, 207, 503
- Helled, R., & Bodenheimer, P. 2011, *Icarus*, in press
- Ida, S., & Lin, D. N. C. 2005, *ApJ*, 626, 1045
- Inutsuka, S.-I., Machida, M. N., & Matsumoto, T. 2010, *ApJ*, 718, L58
- Isella, A., Carpenter, J. M., & Sargent, A. I. 2009, *ApJ*, 701, 260
- Johnson, J. A., et al. 2010, *PASP*, 122, 149
- Kalas, P., et al. 2008, *Science*, 322, 1345
- Lafrenière, D., Jayawardhana, R., & van Kerkwijk, M. H. 2008, *ApJ*, 689, L153
- Lafrenière, D., et al. 2007, *ApJ*, 670, 1367
- Laughlin, G., Bodenheimer, P., & Adams, F. C. 2004, *ApJ*, 612, L73
- Levison, H. F., & Stewart, G. R. 2001, *Icarus*, 153, 224
- Mann, R. K., & Williams, J. P. 2009, *ApJ*, 699, L55
- Mann, R. K., & Williams, J. P. 2010, *ApJ*, 725, 430
- Marois, C., Macintosh, B., Barman, T., Zuckerman, B., Song, I., Patience, J., Lafrenière, D., & Doyon, R. 2008, *Science*, 322, 1348
- Marois, C., Zuckerman, B., Konopacky, Q. M., Macintosh, B., & Barman, T. 2010, *Nature*, 468, 1080

- Mayer, L., Boss, A. P., & Nelson, A. 2010, in *Planets in Binaries*, N. Haghighipour, ed. (New York: Springer), 195
- Mayer, L., Lufkin, G., Quinn, T., & Wadsley, J. 2007, *ApJ*, 661, L77
- Meru, F., & Bate, M. R. 2010, *MNRAS*, 409?, 858
- Meru, F., & Bate, M. R. 2011, *MNRAS*, 410, 559
- Nelsen, A. F. 2006, *MNRAS*, 373, 1039
- Nelsen, A. F., & Benz, W. 2003, *ApJ*, 589, 578
- Nero, D., & Bjorkman, J. E. 2009, *ApJ*, 702, L163
- Nielsen, E. L., et al. 2008, *ApJ*, 674, 466
- Nielsen, E. L., & Close, L. M. 2010, *ApJ*, 717, 878
- Oppenheimer, B. R., et al. 2008, 679, 1574
- Pollack, J. B., Hollenbach, D. J., Beckwith, S., Simonelli, D. P., Roush, T., & Fong, W. 1994, *ApJ*, 421, 615
- Rafikov, R. R. 2005, *ApJ*, 621, L69
- Raymond, S. N., Armitage, P. J., & Gorelick, N. 2010, *ApJ*, 711, 772
- Su, K. Y. L., et al. 2009, *ApJ*, 705, 314
- Spitzer, L. 1968, *Diffuse Matter in Space* (Interscience, New York), p. 216
- Stamatellos, D., & Whitworth, A. P. 2009a, *MNRAS*, 392, 413
- . 2009b, *MNRAS*, 400, 1563
- Thalmann, C., et al. 2009, *ApJ*, 707, L123
- Thommes, E. W., Duncan, M. J., & Levison, H. F. 2002, *AJ*, 123, 2862
- Toomre, A. 1964, *ApJ*, 139, 1217
- Wetherill, G. W. 1996, *Icarus*, 119, 219

Table 1. Initial conditions for the models.

Model	M_s/M_\odot	M_d/M_\odot	M_d/M_s	T_i	T_e	Q_{min}	Q_{max}
2.0	2.0	0.21	0.11	40.	50.	1.13	1.71
1.5	1.5	0.17	0.11	35.	40.	1.12	1.67
1.0	1.0	0.13	0.13	30.	30.	1.13	1.68
0.5	0.5	0.083	0.17	22.	30.	1.12	1.61
0.1	0.1	0.028	0.28	11.	30.	1.11	1.47

Table 2. Fragment properties at time $\sim 4P_{20}$.

Model	M_{disk}/M_{\odot}	M_{frag}/M_{Jup}	a_{frag}/AU	e_{frag}
2.0	0.21	4.6	33.8	0.107
2.0	0.21	2.7	36.7	0.104
2.0	0.21	3.5	37.6	0.106
2.0	0.21	3.5	33.5	0.122
2.0	0.21	4.0	36.4	0.135
2.0	0.21	3.4	35.6	0.149
1.5	0.17	5.1	35.2	0.191
1.5	0.17	4.2	31.2	0.151
1.5	0.17	1.6	32.1	0.077
1.5	0.17	1.8	31.8	0.070
1.0	0.13	2.8	35.1	0.166
1.0	0.13	1.8	32.0	0.119
1.0	0.13	2.9	40.5	0.117
0.5	.083	1.4	43.2	0.174
0.1	.028	.74	48.7	0.350

Table 3. Fragment properties at time $\sim 6P_{20}$.

Model	M_{disk}/M_{\odot}	M_{frag}/M_{Jup}	a_{frag}/AU	e_{frag}
2.0	0.21	1.4	43.	0.019
2.0	0.21	3.1	39.	0.051
2.0	0.21	2.9	43.	0.043
1.5	0.17	4.2	39.	0.19
1.5	0.17	3.0	48.	0.22
1.5	0.17	2.4	41.	0.047
1.5	0.17	4.9	67.	0.22
1.0	0.13	3.0	39.	0.12
1.0	0.13	2.0	37.	0.031
1.0	0.13	3.8	44.	0.11
1.0	0.13	2.5	45.	0.14
0.5	.083	2.1	44.	0.092
0.5	.083	1.9	51.	0.24
0.1	.028	.91	45.	0.33
0.1	.028	.80	42.	0.33

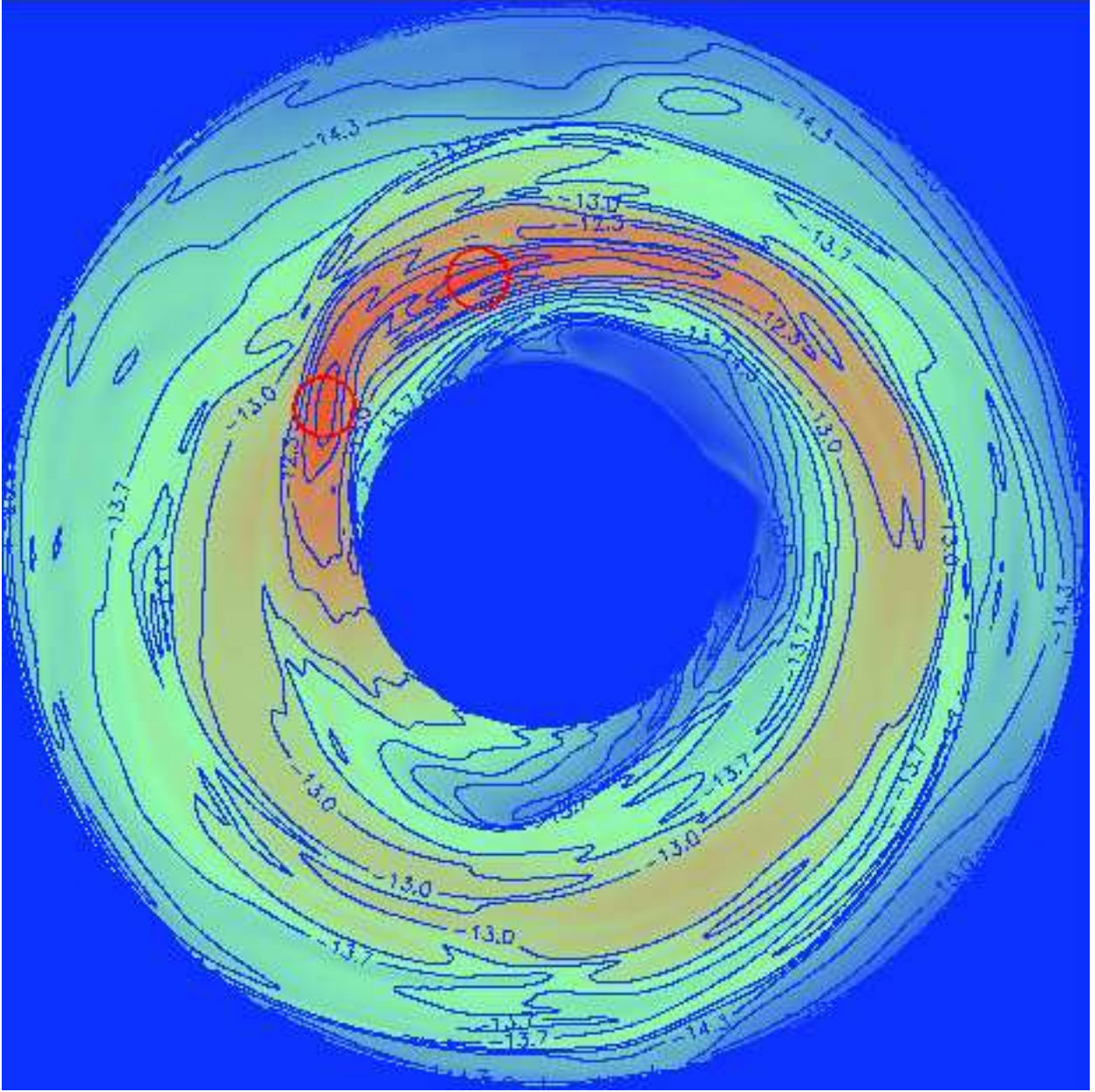


Fig. 1.— Equatorial density contours for model 0.1 after 1843 yr of evolution. In this plot and subsequent density contour plots, each contour represents a change in density by factor of about 2. The disk has an inner radius of 20 AU and an outer radius of 60 AU. Red circles denote the fragments listed in Table 3.

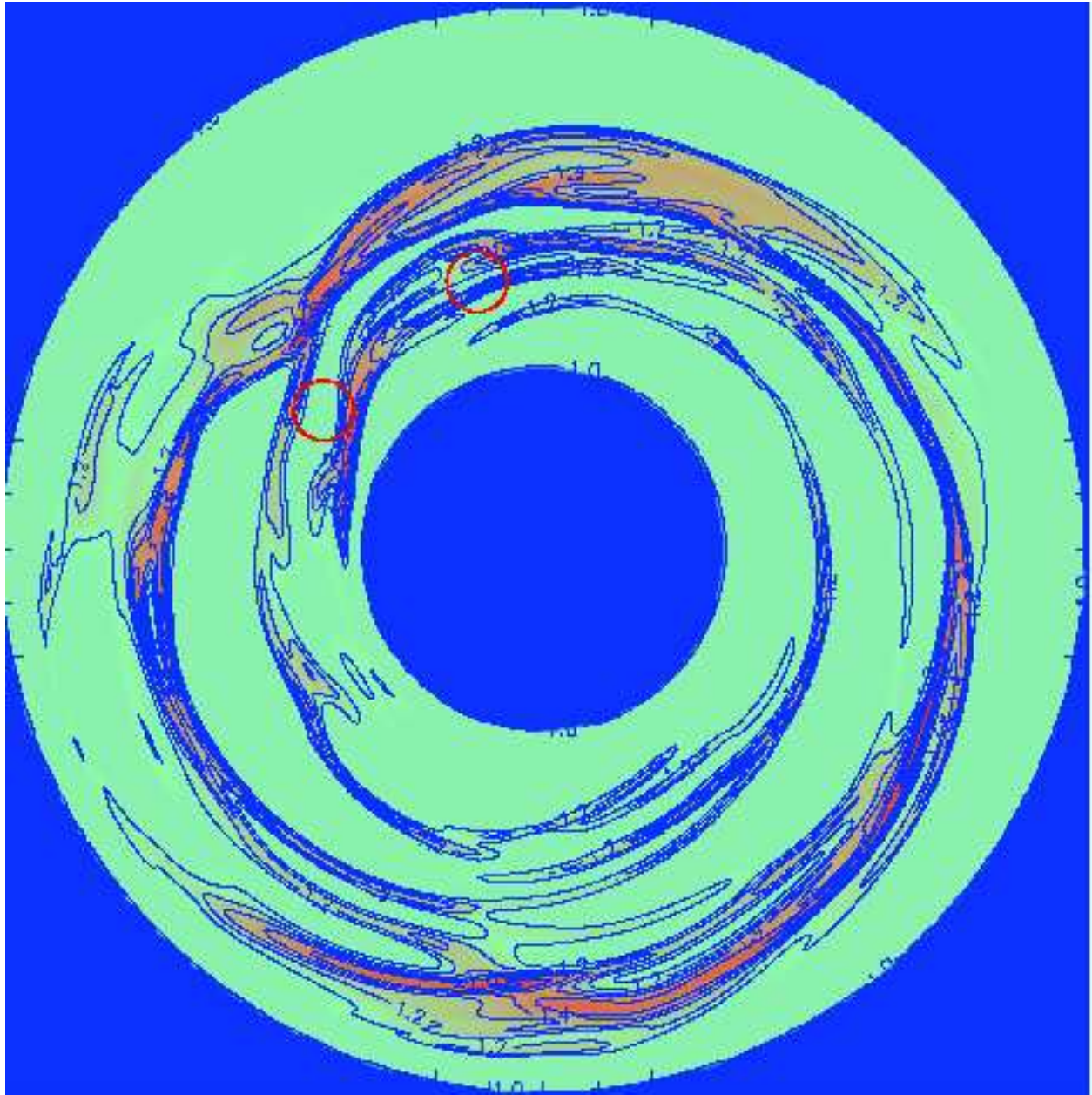


Fig. 2.— Equatorial temperature contours for model 0.1 after 1843 yr of evolution. In this plot and subsequent temperature contour plots, each contour represents a change in temperature by a factor of about 1.3.

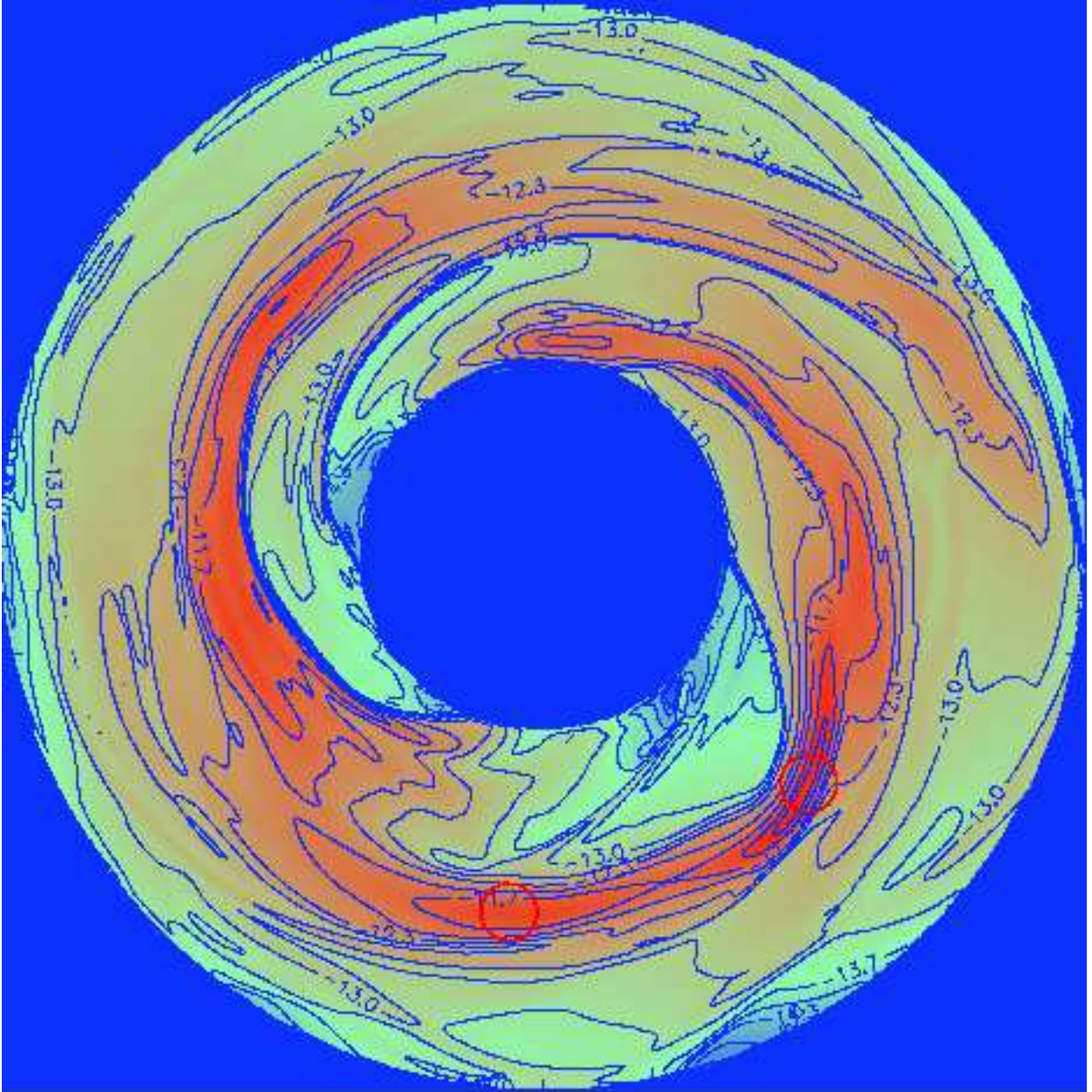


Fig. 3.— Equatorial density contours for model 0.5 after 771 yr of evolution.

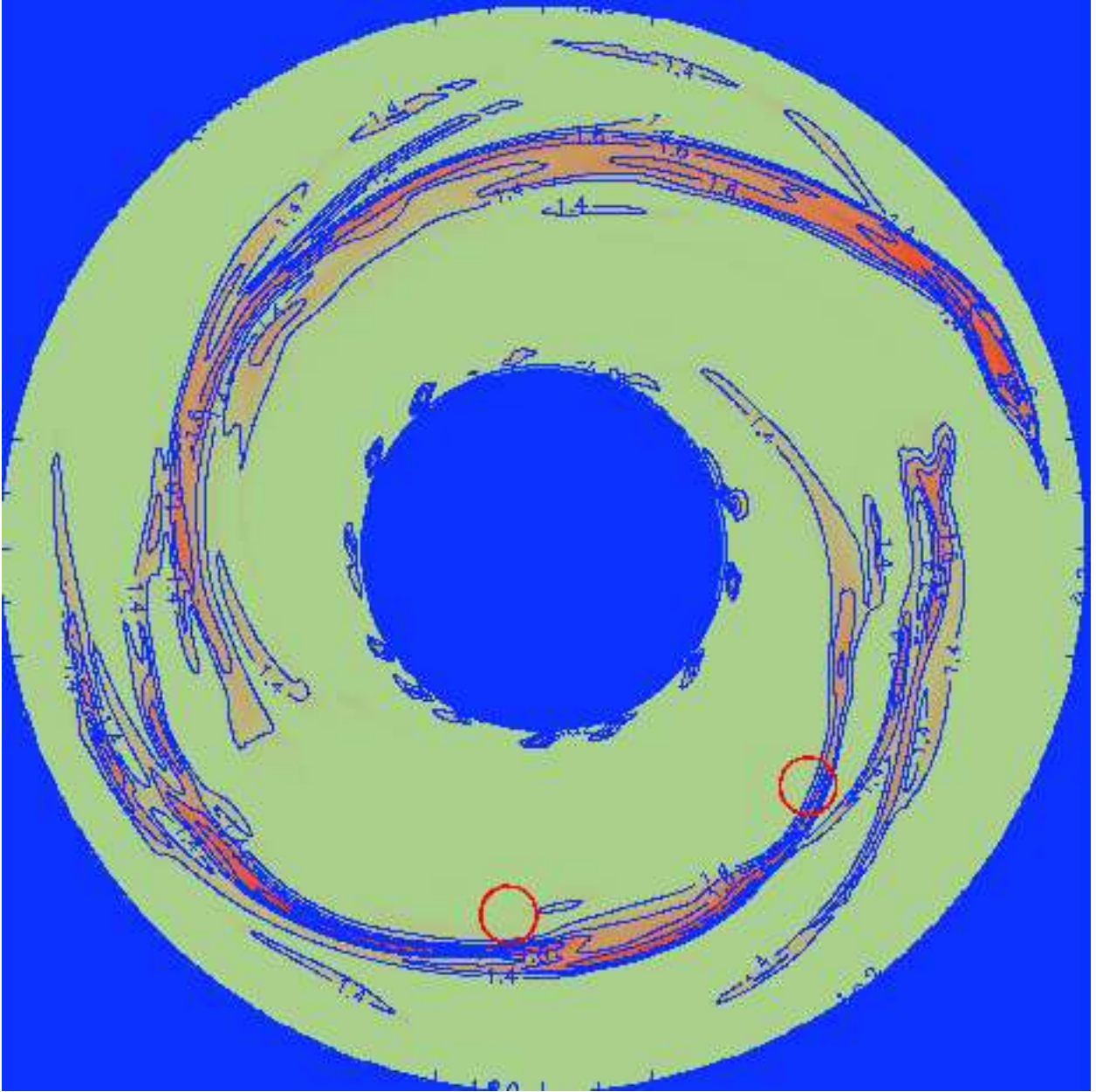


Fig. 4.— Equatorial temperature contours for model 0.5 after 771 yr of evolution.

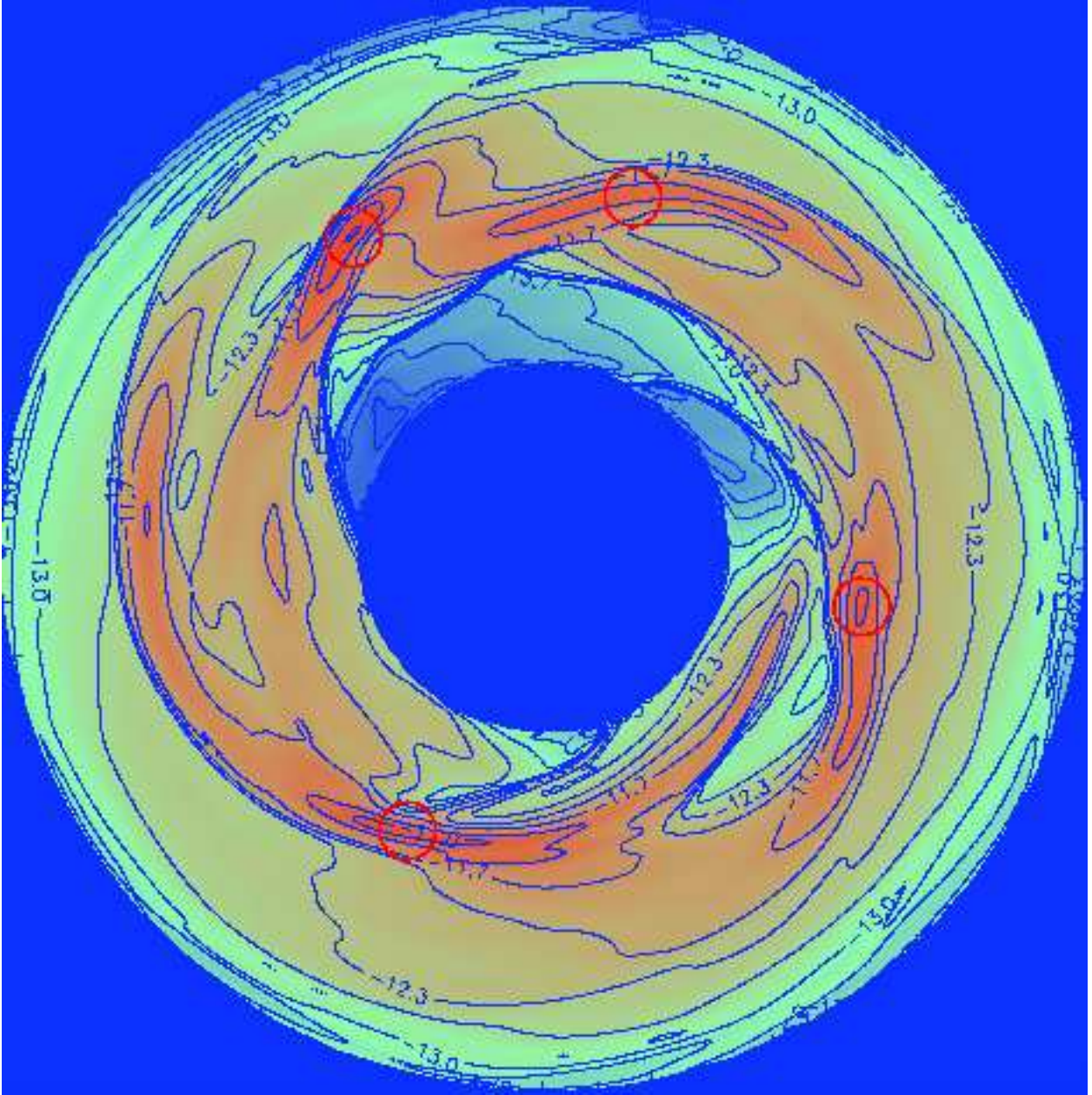


Fig. 5.— Equatorial density contours for model 1.0 after 547 yr of evolution.

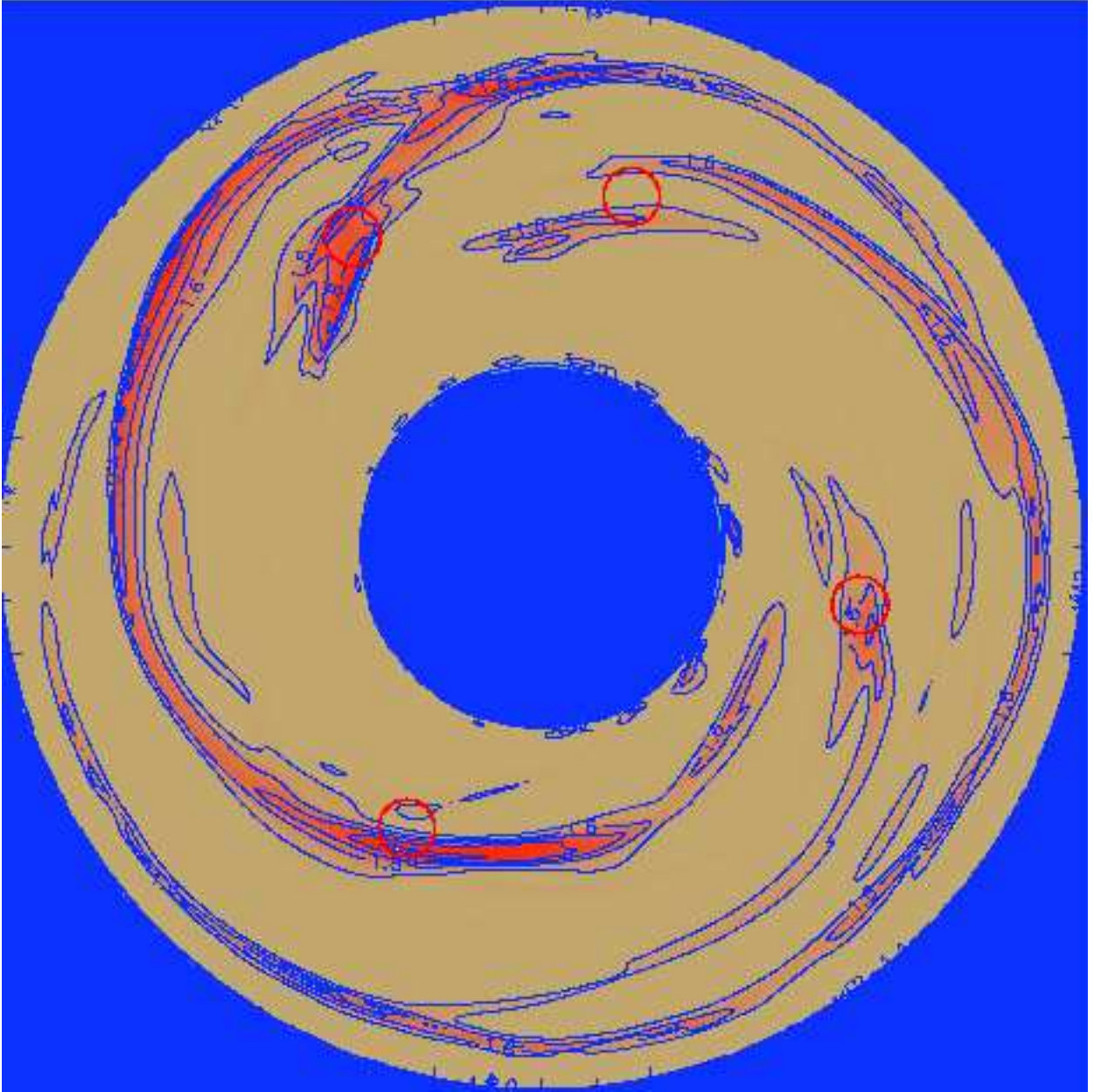


Fig. 6.— Equatorial temperature contours for model 1.0 after 547 yr of evolution.

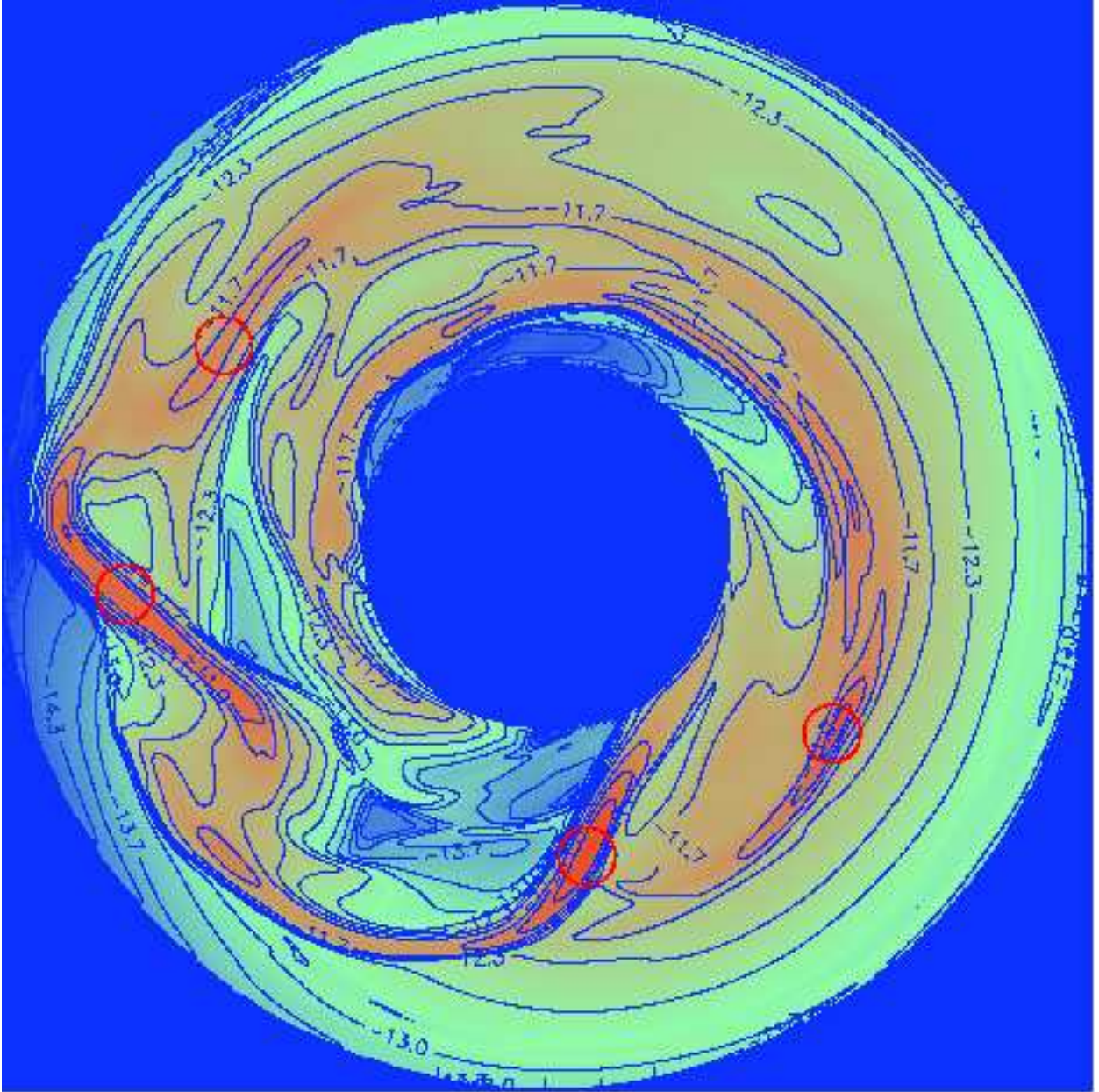


Fig. 7.— Equatorial density contours for model 1.5 after 446 yr of evolution.

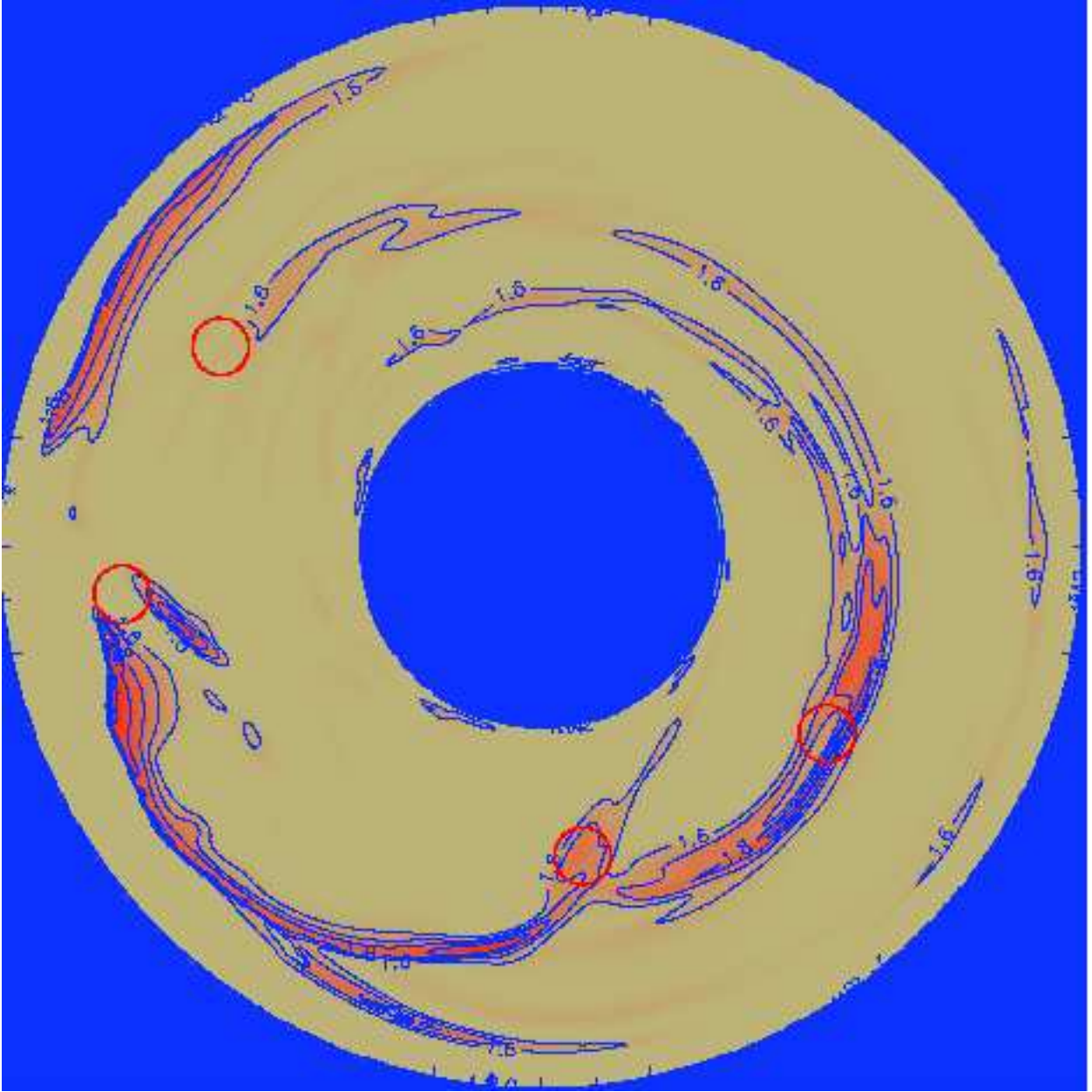


Fig. 8.— Equatorial temperature contours for model 1.5 after 446 yr of evolution.

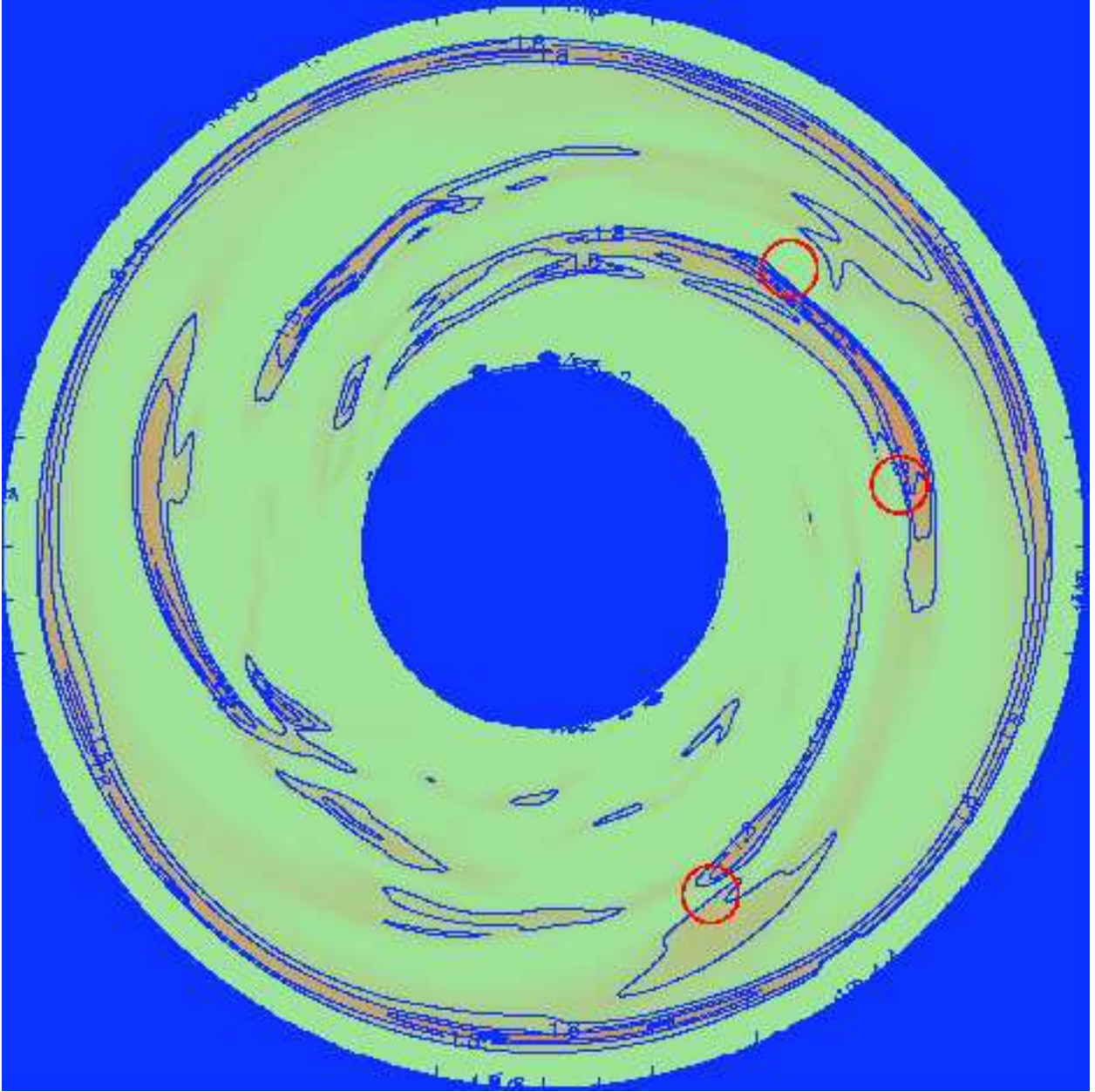


Fig. 10.— Equatorial temperature contours for model 2.0 after 387 yr of evolution.

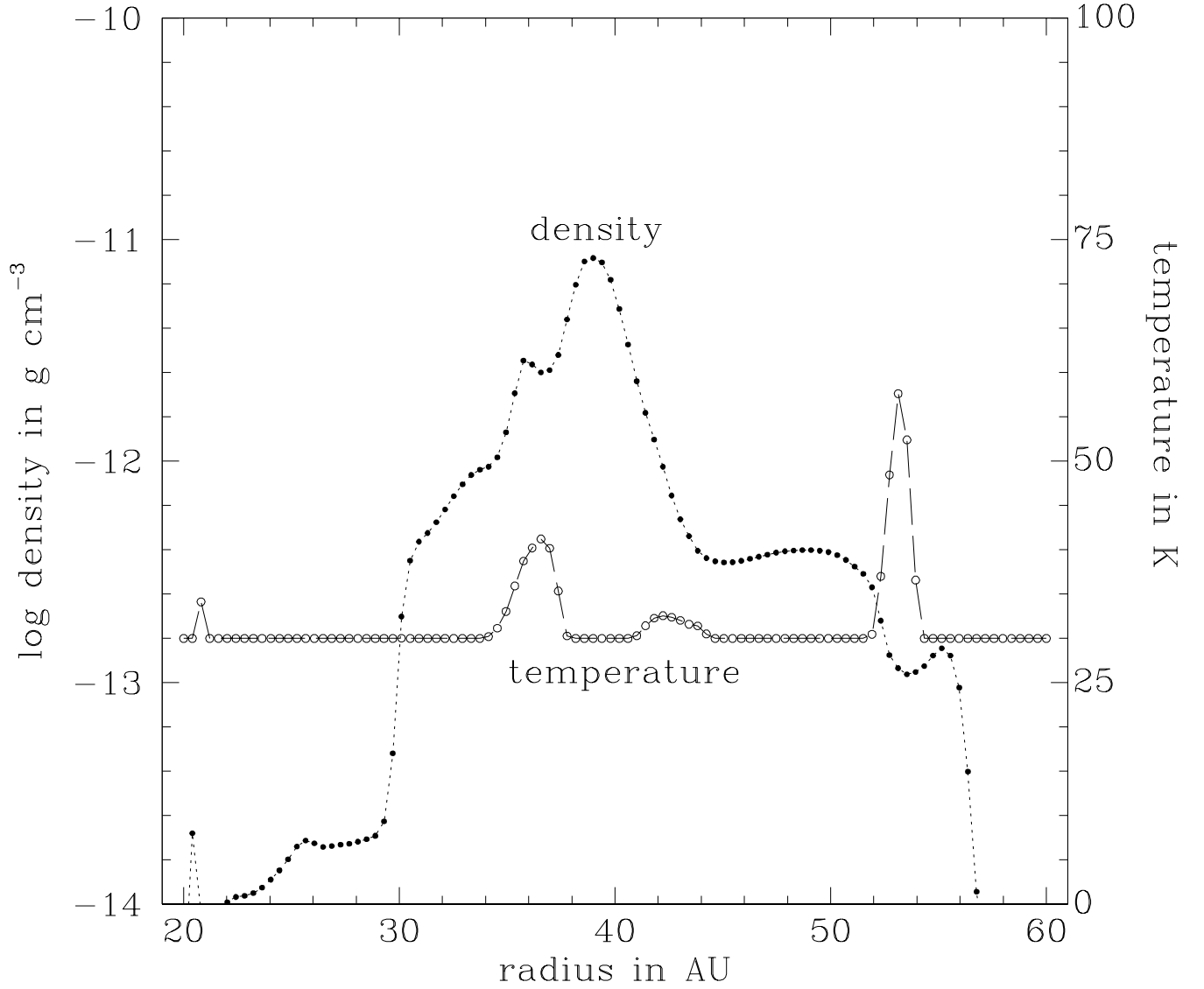


Fig. 11.— Midplane density and temperature radial profiles for the clump at 12 midnight in Figures 5 and 6 for model 1.0.

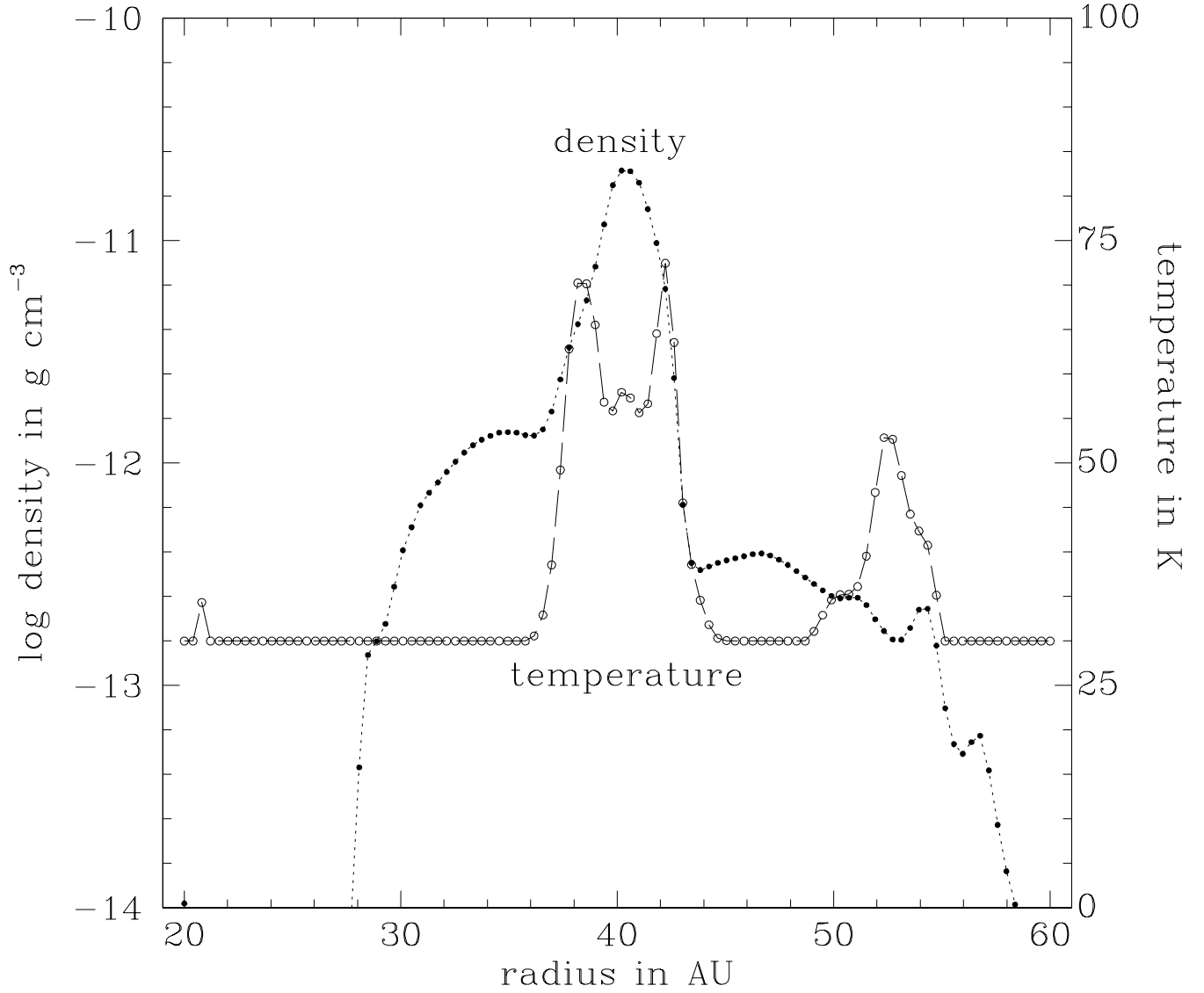


Fig. 12.— Midplane density and temperature radial profiles for the clump at 11 o'clock in Figures 5 and 6 for model 1.0.

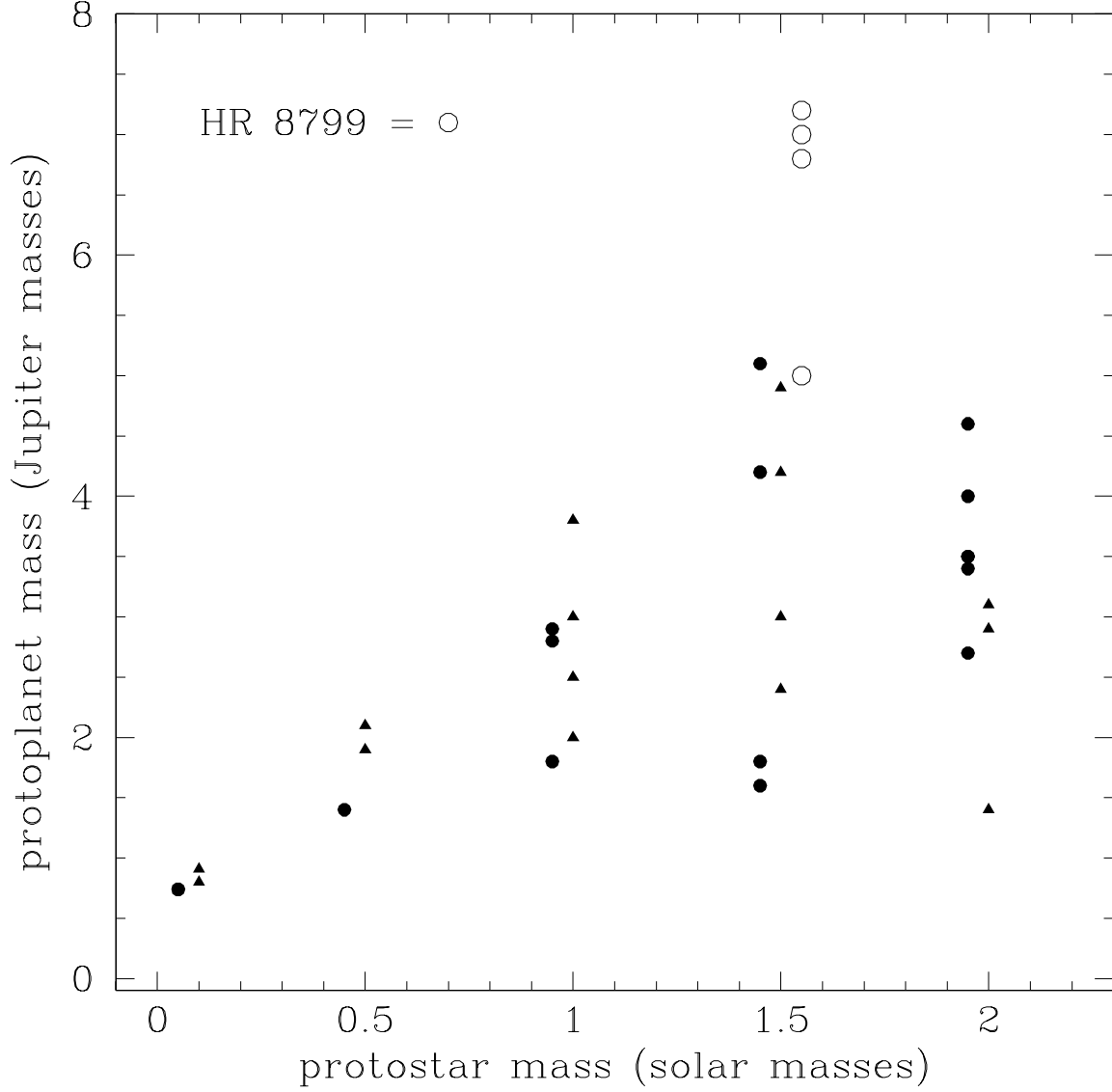


Fig. 13.— Protoplanet masses as a function of protostellar mass, compared to estimated planet masses for the HR 8799 system (Marois et al. 2008, 2010), assuming an age of 30 Myr for HR 8799. In this plot and the subsequent plots, filled circles represent estimated protoplanet properties at a time of $\sim 4P_{20}$, while filled triangles represent the estimates at a time of $\sim 6P_{20}$. The nominal protostellar masses for the filled circles have been shifted slightly to the left for clarity, while those for HR 8799 have been shifted to the right, as well as up and down in mass for the three $7 M_{Jup}$ planets.

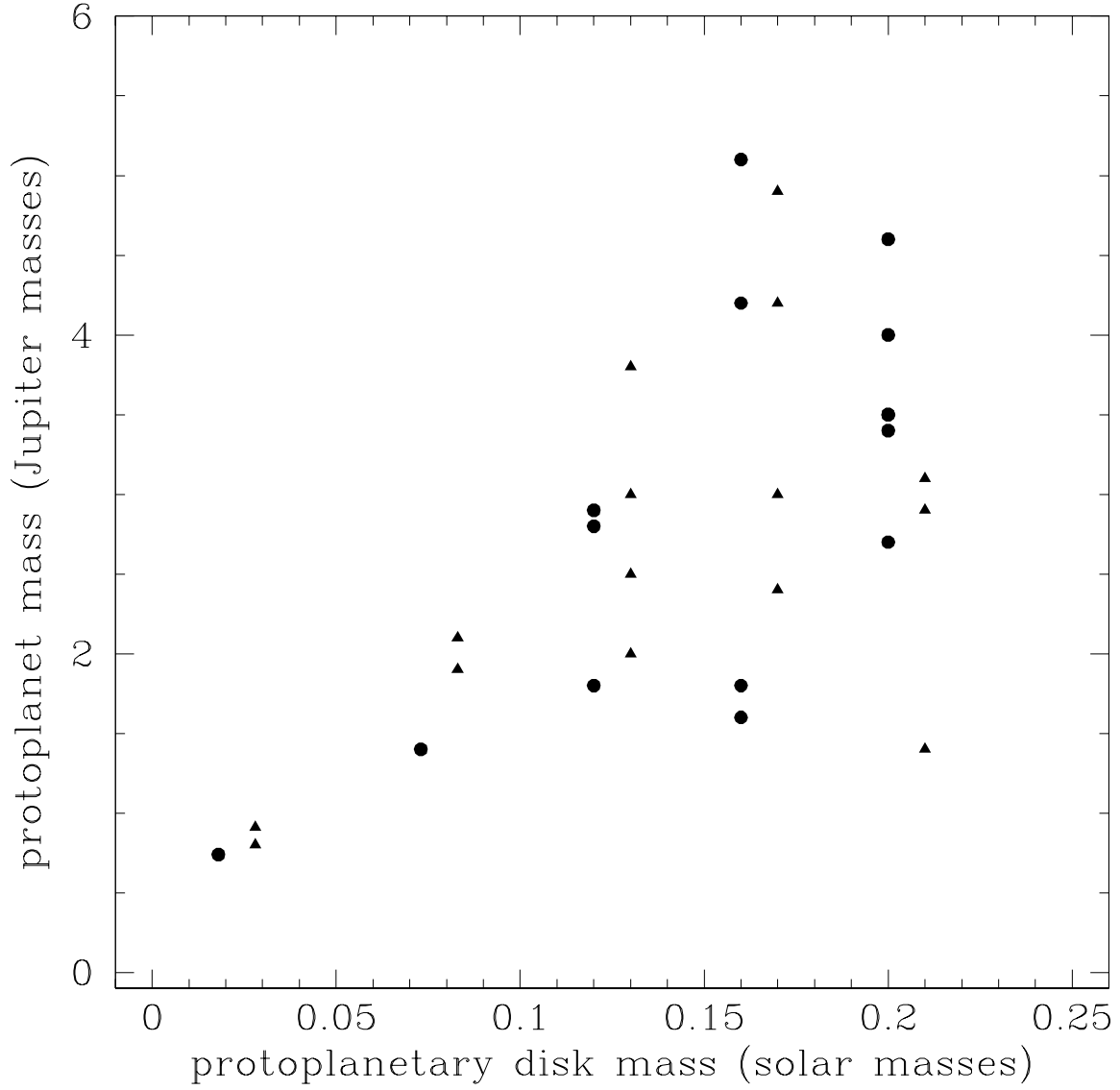


Fig. 14.— Protoplanet masses as a function of protoplanetary disk mass. Filled circles have been shifted to the left for clarity.

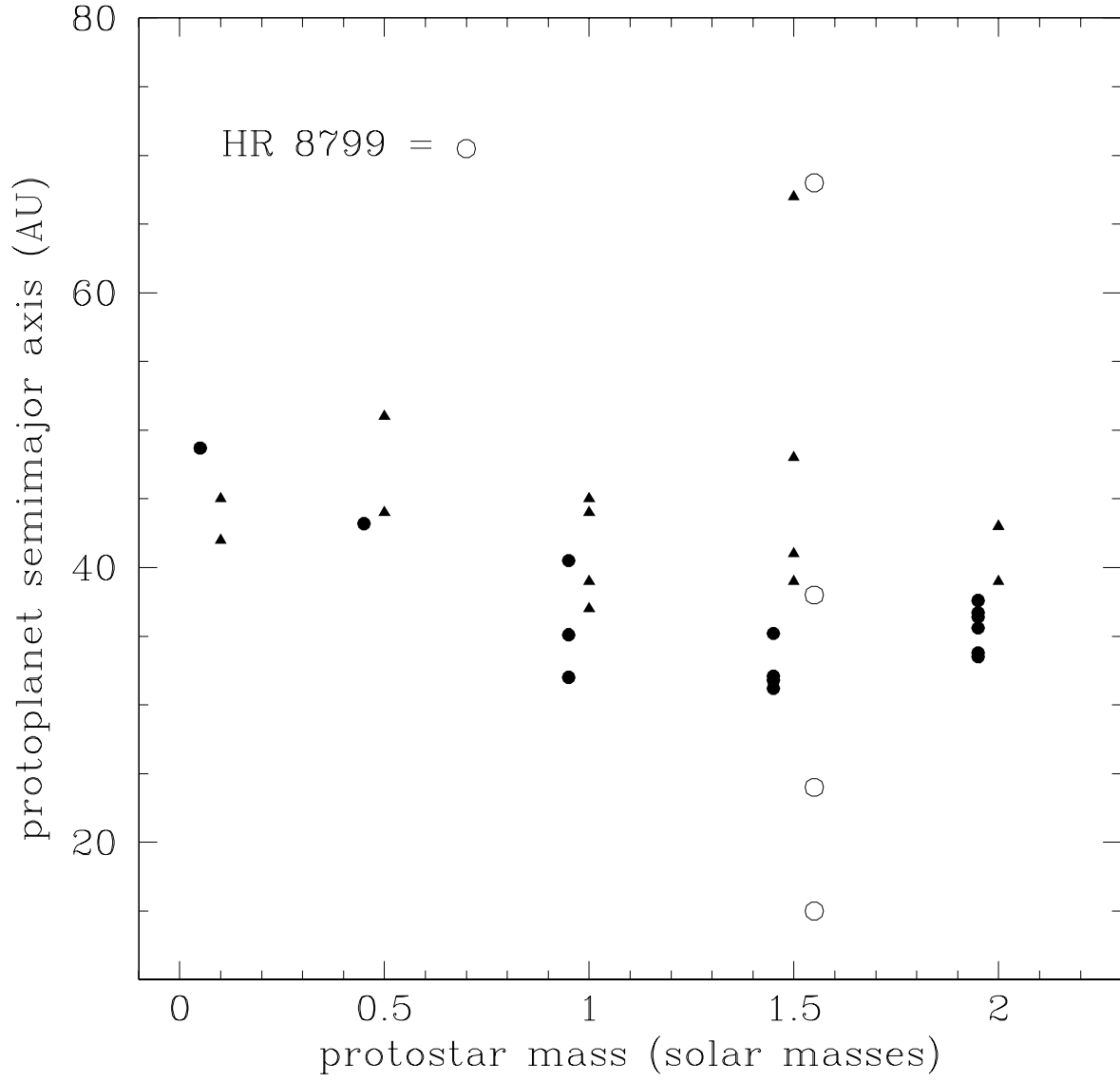


Fig. 15.— Protoplanet orbital semimajor axes as a function of protostellar mass.

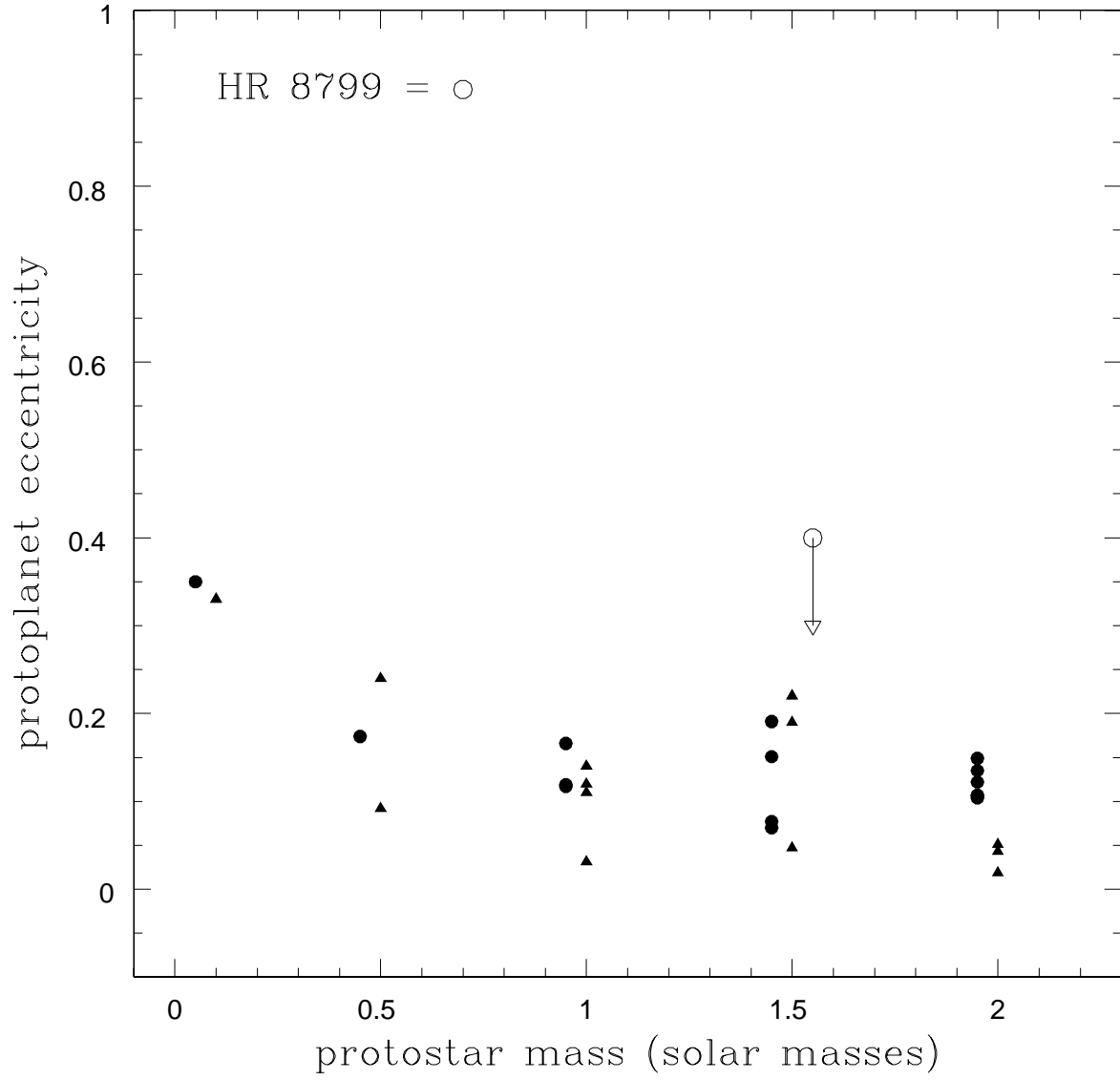


Fig. 16.— Protoplanet orbital eccentricities as a function of protostellar mass.